INTERNATIONAL JOURNAL FOR NUMERICAL METHODS IN FLUIDS, VOL. 13, 557–578 (1991)

EVALUATION OF THE DRAG FORCE BY INTEGRATING THE ENERGY DISSIPATION RATE IN STOKES FLOW FOR 2D DOMAINS USING THE FEM

RAM K. GANESH

Department of Mechanical Engineering, University of Connecticut, Storrs, CT 06268, U.S.A.

SUMMARY

The total drag force on the surface of a body, which is the sum of the form drag and the skin friction drag in a 2D domain, is numerically evaluated by integrating the energy dissipation rate in the whole domain for an incompressible Stokes fluid. The finite element method is used to calculate both the energy dissipation rate in the whole domain as well as the drag on the boundary of the body. The evaluation of the drag and the energy dissipation rate are post-processing operations which are carried out after the velocity field and the pressure field for the flow over a particular profile have been obtained. The results obtained for the flow over three different but constant area profiles —a circle, an ellipse and a cross-section of a prolate spheroid—with uniform inlet velocity are presented and it is shown that the total drag force times the velocity is equal to the total energy dissipation rate in the entire finite flow domain. Hence, by calculating the energy dissipation rate in the domain with unit velocity specified at the far-field boundary enclosing the domain, the drag force on the boundary of the body can be obtained.

KEY WORDS Drag Energy dissipation rate Stokes law Finite domain Stress-divergence Outflow boundary conditions

1. INTRODUCTION

In fluid dynamics, the fluid-dynamic resistance or the aerodynamic drag on a body in an external flow condition can be evaluated analytically, only for a few idealized cases,[1] such as flow over a sphere with uniform velocity at infinity and experimentally for a multitude of bodies.[2] It is now possible, with the advent of computing machinery and with the aid of a suitable numerical method such as the finite element method, to numerically solve for the velocity and pressure fields for the flow over an arbitrary body. Having solved for the velocity and pressure fields successfully, subroutine subprogrammes can be developed which can evaluate both the drag force on the boundary of the arbitrary body and the total energy dissipation rate for the entire domain. Two such subroutines were developed and used here to numerically verify *Stokes' law in 2D* and to use this as a means to numerically obtain the drag from the energy dissipation rate. It is worth pointing out that the minimum drag problem in Stokes flow, which is treated as an optimal control problem for a distributed parameter system governed by linear elliptic partial differential equation with the control as the geometric element of the system, actually uses the energy dissipation rate as the cost function to be minimized.[3]

It is to be noted that for 2D Stokes flow over a circular profile there exists no solution that can satisfy no-slip on the profile yet can have finite velocity at inifinity. This is not the case, however

0271–2091/91/150557–22$11.00

Received 22 February 1988
Revised 16 November 1990

for 3D Stokes flow past a sphere. This situation is sometimes referred to as the 'Stokes paradox' in the literature.[4] In this paper Stokes flow over three different profiles in 2D is solved numerically and the Stokes drag law in 2D is verified (despite the presence of the Stokes paradox); this result is subsequently used to obtain the drag on the profile.

2. THEORETICAL BACKGROUND

For a *Stokes* fluid the constitutive equation (stress, rate of strain relationship) is

$$\sigma_{ij} = -p\delta_{ij} + 2\mu V_{ij} - \tfrac{2}{3}\mu V_{kk}\delta_{ij}, \tag{1}$$

where σ_{ij} is the stress tensor, μ is the dynamic viscosity, V_{ij} is the rate of deformation tensor, V_{kk} is the rate of dilation tensor and p is the static pressure. If the fluid is assumed incompressible, then V_{kk} is zero and the constitutive equation becomes

$$\sigma_{ij} = -p\delta_{ij} + 2\mu V_{ij}, \tag{2}$$

where

$$V_{ij} = \tfrac{1}{2}(v_{i,j} + v_{j,i}).$$

The normal stress can be found by setting $i=j$:

$$\begin{aligned}\sigma_{ii} &= -p\delta_{ii} + 2\mu V_{ii} \quad \text{(summation not implied)} \\ &= -p + 2\mu\frac{\partial v_i}{\partial x_i},\end{aligned} \tag{3}$$

and the shear stress is given by

$$\sigma_{ij} = \mu\left(\frac{\partial v_i}{\partial x_j} + \frac{\partial v_j}{\partial x_i}\right). \tag{4}$$

In 2D Cartesian co-ordinates, the normal and shear stresses can be written as

$$\sigma_{xx} = -p + 2\mu\frac{\partial u}{\partial x}, \tag{5}$$

$$\sigma_{xy} = \mu\left(\frac{\partial u}{\partial y} + \frac{\partial v}{\partial x}\right). \tag{6}$$

2.1. Drag

Assuming the flow velocity U_∞ to be in the x-direction (with the associated unit vector $\hat{\mathbf{i}}$), the component of the stress vector acting on a surface with unit normal v in the x-direction is given by the Cauchy formula[5]

$$T_x^v = \sigma_{xx}\, l + \sigma_{yx}\, m, \tag{7}$$

where σ_{xx} and σ_{yx} are the normal and shear stresses respectively. The direction cosines are l and m. The above formula gives the drag at a point on a boundary. The total drag force D in the x-direction is obtained by integrating this expression along the boundary of the body:

$$\begin{aligned}D &= \int_\Gamma (\sigma_{xx}\, l + \sigma_{xy}\, m)\, \mathrm{d}\Gamma \\ &= \int_\Gamma \left[\left(-p + 2\mu\frac{\partial u}{\partial x}\right) l + \mu\left(\frac{\partial v}{\partial x} + \frac{\partial u}{\partial y}\right) m\right] \mathrm{d}\Gamma.\end{aligned} \tag{8}$$

2.2. Energy dissipation rate

The energy dissipation function in 2D in tensor notation is given by

$$\phi = \tfrac{1}{2}(v_{i,j} + v_{j,i})^2. \tag{9}$$

In Cartesian co-ordinates this becomes[1]

$$\phi = 2\left[\left(\frac{\partial u}{\partial x}\right)^2 + \left(\frac{\partial v}{\partial y}\right)^2 + \frac{1}{2}\left(\frac{\partial u}{\partial y} + \frac{\partial v}{\partial x}\right)^2\right]. \tag{10}$$

The energy dissipation rate Φ is the product of dynamic viscosity μ and energy dissipation function ϕ.

2.3. The connection between drag and energy dissipation rate

The Stokes equation in stress-divergence form and the continuity equation are

$$\nabla \cdot \boldsymbol{\Pi} = \nabla p, \tag{11}$$

where

$$\Pi_{ij} = \mu(v_{i,j} + v_{j,i}), \tag{11a}$$

and

$$\nabla \cdot \mathbf{U} = 0. \tag{12}$$

Expressing the momentum equation differently, we get

$$\nabla \cdot (\boldsymbol{\Pi} - p\boldsymbol{I}) = 0, \tag{13}$$

where $\boldsymbol{I}$ is the unit tensor. Integrating this over the entire domain Ω gives

$$\int_\Omega \nabla \cdot (\boldsymbol{\Pi} - p\boldsymbol{I})\, d\Omega = 0. \tag{14}$$

Using Gauss's theorem, equation (14) becomes

$$\int_\Gamma (\boldsymbol{\sigma} \cdot \hat{\mathbf{n}})\, d\Gamma = 0, \tag{15}$$

where

$$\boldsymbol{\sigma} \cdot \hat{\mathbf{n}} = \boldsymbol{\Pi} \cdot \hat{\mathbf{n}} - p\hat{\mathbf{n}} \tag{15a}$$

and Γ is the 'finite' boundary of the fluid domain.

Now, let Γ_0 be the boundary of the body over which the drag is to be obtained and Γ_{inlet}, Γ_{top}, Γ_{symm} and Γ_{exit} be the other boundaries of the finite domain (see Figure 1), which together enclose a large volume of fluid. With this definition of the boundaries equation (15) becomes

$$\int_{\Gamma_0} (\boldsymbol{\sigma} \cdot \hat{\mathbf{n}})\, d\Gamma + \int_{\Gamma_{inlet}} (\boldsymbol{\sigma} \cdot \hat{\mathbf{n}})\, d\Gamma + \int_{\Gamma_{top}} (\boldsymbol{\sigma} \cdot \hat{\mathbf{n}})\, d\Gamma + \int_{\Gamma_{symm}} (\boldsymbol{\sigma} \cdot \hat{\mathbf{n}})\, d\Gamma + \int_{\Gamma_{exit}} (\boldsymbol{\sigma} \cdot \hat{\mathbf{n}})\, d\Gamma = 0. \tag{16}$$

The total reactive force $\mathbf{F}$ exerted by the body on the fluid is

$$\mathbf{F} = \int_{\Gamma_0} (\boldsymbol{\sigma} \cdot \hat{\mathbf{n}})\, d\Gamma. \tag{17}$$

Therefore it follows from equations (16) and (17) that

$$\mathbf{F} = -\int_{\Gamma_{inlet}} (\boldsymbol{\sigma} \cdot \hat{\mathbf{n}})\, d\Gamma - \int_{\Gamma_{top}} (\boldsymbol{\sigma} \cdot \hat{\mathbf{n}})\, d\Gamma - \int_{\Gamma_{symm}} (\boldsymbol{\sigma} \cdot \hat{\mathbf{n}})\, d\Gamma - \int_{\Gamma_{exit}} (\boldsymbol{\sigma} \cdot \hat{\mathbf{n}})\, d\Gamma. \tag{18}$$

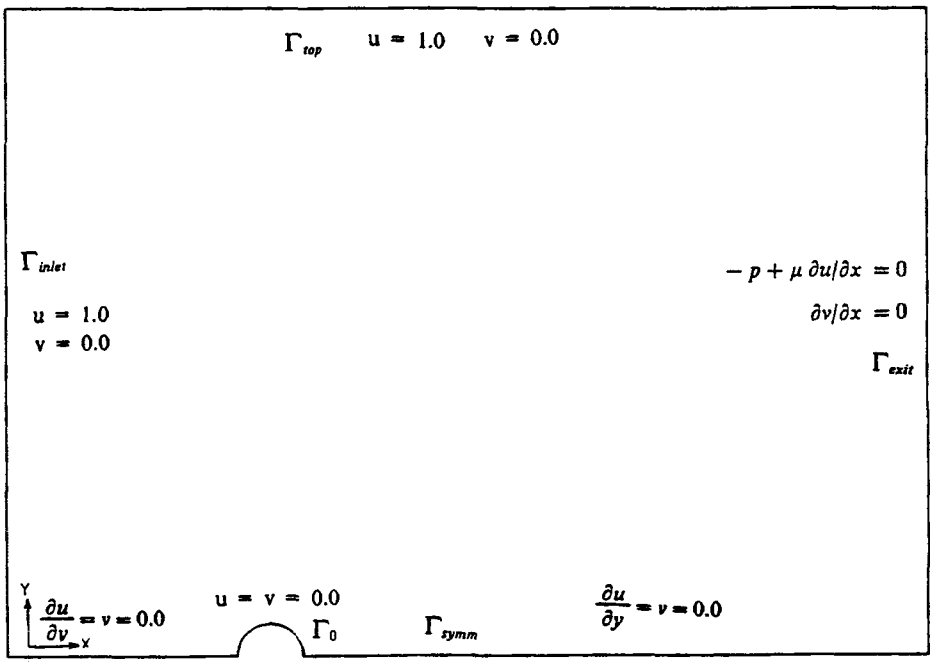

Figure 1. Flow domain with boundary conditions

This equation implies that since **F** is not zero (even when the boundaries are at infinity), the sum of the integral terms associated with them is not zero. It also provides an alternative way to evaluate the drag involving a finite domain boundary, which is normally chosen to be parallel to the global (x, y)-axes. The rate of work done by the boundary force on the fluid at a point is obtained by forming the dot product of that force with the velocity vector at the same point. Therefore the total rate of work done by the boundary forces is obtained by integrating the vector dot product at a point along the boundary. Thus the total rate of work $W_{\mathbf{F}}$ done by the boundary forces comprising **F** is

$$W_{\mathbf{F}} = -\int_{\Gamma_{\text{inlet}}} (\boldsymbol{\sigma}\cdot\hat{\mathbf{n}})\cdot\mathbf{U}_\infty \, d\Gamma - \int_{\Gamma_{\text{top}}} (\boldsymbol{\sigma}\cdot\hat{\mathbf{n}})\cdot\mathbf{U}_\infty \, d\Gamma$$
$$-\int_{\Gamma_{\text{symm}}} (\boldsymbol{\sigma}\cdot\hat{\mathbf{n}})\cdot\mathbf{U}_{\text{symm}} \, d\Gamma - \int_{\Gamma_{\text{exit}}} (\boldsymbol{\sigma}\cdot\hat{\mathbf{n}})\cdot\mathbf{U}_{\text{exit}} \, d\Gamma. \tag{19}$$

Expanding the integrands to show the tractions and the direction cosines, we get

$$W_{\mathbf{F}} = -\int_{\Gamma_{\text{inlet}}} u_\infty(\sigma_{xx}n_x + \sigma_{xy}\overset{0}{\overset{\nearrow}{n_y}}) \, d\Gamma - \int_{\Gamma_{\text{inlet}}} \overset{0}{\overset{\nearrow}{v}}(\sigma_{yx}n_x + \sigma_{yy}\overset{0}{\overset{\nearrow}{n_y}}) \, d\Gamma$$
$$-\int_{\Gamma_{\text{top}}} u_\infty(\sigma_{xx}\overset{0}{\overset{\nearrow}{n_x}} + \sigma_{xy}n_y) \, d\Gamma - \int_{\Gamma_{\text{top}}} \overset{0}{\overset{\nearrow}{v}}(\sigma_{yx}\overset{0}{\overset{\nearrow}{n_x}} + \sigma_{yy}n_y) \, d\Gamma$$

$$-\int_{\Gamma_{symm}} u(\sigma_{xx}\overset{0}{\nearrow}n_x+\sigma_{xy}\overset{0}{\nearrow}n_y)\,d\Gamma-\int_{\Gamma_{symm}} v(\sigma_{yx}\overset{0}{\nearrow}n_x+\sigma_{yy}\overset{0}{\nearrow}n_y)\,d\Gamma$$

$$-\int_{\Gamma_{exit}} u(\overset{0}{\nearrow}\sigma_{xx}n_x+\overset{0}{\nearrow}\sigma_{xy}n_y)\,d\Gamma-\int_{\Gamma_{exit}} v(\overset{0}{\nearrow}\sigma_{yx}n_x+\overset{0}{\nearrow}\sigma_{yy}n_y)\,d\Gamma, \tag{20}$$

where the terms 'zeroed out' via the arrows will be discussed below.

It may be noted that the boundary conditions in the Stokes formulation of Figure 1 do not represent the stresses physically, even though from a numerical standpoint, it does not make much difference as far as solving for the flow field is concerned. The numerical result obtained by employing the Stokes formulation and the associated outflow gradient velocity boundary conditions would be nearly the same (the small difference that results is due to a difference in truncation error) as that would be obtained by employing the stress-divergence formulation and the associated outflow stress boundary conditions, namely $\sigma_{xx}=0$ and $\sigma_{yx}=0$ (see Appendix I). Once the numerical flow field has been obtained by either method, the stress on any boundary can be calculated as a post-processing operation using the appropriate formula (such as equation (8)) which represents the stress (force) physically.

Now, as a result of the boundary conditions and the orientations of the boundaries, equation (20) reduces to

$$\begin{aligned} W_{\mathbf{F}} &= -\int_{\Gamma_{inlet}} u_\infty(-\sigma_{xx})\,d\Gamma-\int_{\Gamma_{top}} u_\infty(\sigma_{xy})\,d\Gamma \\ &= \mathbf{F}\cdot\mathbf{U}_\infty \\ &= U_\infty D, \end{aligned} \tag{21}$$

where 'D' is the x-component of the total reactive force $\mathbf{F}$. Since 'Drag' is defined as the force component parallel to the relative approach velocity exerted on the body by the moving fluid, 'D' here is the reaction to 'Drag' exerted by the body on the fluid.

Next, by considering the total rate of work done by the boundary forces, it will be shown that an existing result in the literature is obtained in a different Galilean reference frame:

$$\int_\Gamma(\boldsymbol{\sigma}\cdot\hat{\mathbf{n}})\cdot\mathbf{U}_\Gamma\,d\Gamma=\int_{\Gamma_0}(\boldsymbol{\sigma}\cdot\hat{\mathbf{n}})\cdot\mathbf{U}_0\,d\Gamma+\int_{\Gamma_{inlet}}(\boldsymbol{\sigma}\cdot\hat{\mathbf{n}})\cdot\mathbf{U}_\infty\,d\Gamma$$

$$+\int_{\Gamma_{top}}(\boldsymbol{\sigma}\cdot\hat{\mathbf{n}})\cdot\mathbf{U}_\infty\,d\Gamma+\int_{\Gamma_{symm}}(\boldsymbol{\sigma}\cdot\hat{\mathbf{n}})\cdot\mathbf{U}_{symm}\,d\Gamma+\int_{\Gamma_{exit}}(\boldsymbol{\sigma}\cdot\hat{\mathbf{n}})\cdot\mathbf{U}_{exit}\,d\Gamma, \tag{22}$$

where the RHS is obtained by marking the boundaries as done before for the forces. Applying Gauss theorem, the LHS integral becomes

$$\int_\Gamma(\boldsymbol{\sigma}\cdot\hat{\mathbf{n}})\cdot\mathbf{U}_\Gamma\,d\Gamma=\int_\Omega\nabla\cdot(\boldsymbol{\sigma}\cdot\mathbf{U})\,d\Omega, \tag{23}$$

where $\mathbf{U}$ is the velocity vector inside the domain at any point.

If the body is assumed stationary, the velocity $\mathbf{U}_0$ on the boundary Γ_0 of the body is a null vector owing to the no-slip condition and hence the first integral term on the RHS of equa-

tion (22) vanishes. Therefore equation (23), by virtue of equations (22), (20) and (21), becomes

$$\int_\Omega \nabla\cdot(\boldsymbol{\sigma}\cdot\mathbf{U})\,d\Omega = -W_F$$
$$= -U_\infty D. \tag{24}$$

From vector calculus we know the following:

$$\nabla\cdot(\boldsymbol{\Pi}\cdot\mathbf{U}) = \mathbf{U}\cdot(\nabla\cdot\boldsymbol{\Pi}) + \boldsymbol{\Pi}:\nabla\mathbf{U}, \tag{25a}$$

$$\nabla\cdot(\mathbf{U}p) = p(\nabla\cdot\mathbf{U}) + \mathbf{U}\cdot\nabla p. \tag{25b}$$

Invoking conservation of mass, $\nabla\cdot\mathbf{U}=0$, the first term on the RHS of equation (25b) goes to zero. Now, subtracting equation (25b) from equation (25a), the LHS integral in equation (24) becomes

$$\int_\Omega \nabla\cdot(\boldsymbol{\Pi}\cdot\mathbf{U} - p\mathbf{U})\,d\Omega = \int_\Omega \nabla\cdot(\boldsymbol{\sigma}\cdot\mathbf{U})\,d\Omega$$
$$= \int_\Omega \boldsymbol{\Pi}:\nabla\mathbf{U}\,d\Omega + \int_\Omega \mathbf{U}\cdot(\nabla\cdot\boldsymbol{\Pi} - \nabla p)\,d\Omega. \tag{26}$$

The second integral on the RHS is zero by virtue of equation (11), and the integrand in the first integral on the RHS can be shown to be the energy dissipation rate Φ described in Section 2.2. Therefore from equations (24) and (26) it follows that

$$-U_\infty D = \int_\Omega \Phi\,d\Omega. \tag{27}$$

This agrees with the results obtained by Bird *et al.*,[1] Panton[6] and Serrin.[7] The difference between the approach by these authors and the one given here is in the definition of the coordinate reference frame. Here the body is considered to be stationary while the stream flows past it, with the result that the velocity on the boundary of the body is zero and the velocity sufficiently far away from the body is $\mathbf{U}_\infty$. On the other hand, if the body is considered to be moving through the fluid slowly, the velocity on the boundary of the body is $\mathbf{U}$, which is the translational velocity of the body, and the velocity sufficiently far away from the body in a quiescent state is zero.

3. FIELD EQUATIONS

The conservation of mass and conservation of momentum (the Stokes equation) for incompressible flow are

$$\frac{\partial u}{\partial x} + \frac{\partial v}{\partial y} = 0, \tag{28}$$

$$0 = \mu\left(\frac{\partial^2 u}{\partial x^2} + \frac{\partial^2 u}{\partial y^2}\right) - \frac{\partial p}{\partial x}, \qquad 0 = \mu\left(\frac{\partial^2 v}{\partial x^2} + \frac{\partial^2 v}{\partial y^2}\right) - \frac{\partial p}{\partial y}. \tag{29}$$

Defining the non-dimensionalized variables to be

$$u^* = u/u_\infty, \qquad v^* = v/u_\infty, \qquad p^* = p/(u_\infty \mu_{ref}/r),$$
$$x^* = x/r, \qquad y^* = y/r, \qquad \mu^* = \mu/\mu_{ref}, \tag{30}$$

the non-dimensionalized equations become (dropping the asterisks)

$$\frac{\partial u}{\partial x}+\frac{\partial v}{\partial y}=0, \tag{31}$$

$$0=\mu\left(\frac{\partial^2 u}{\partial x^2}+\frac{\partial^2 u}{\partial y^2}\right)-\frac{\partial p}{\partial x}, \qquad 0=\mu\left(\frac{\partial^2 v}{\partial x^2}+\frac{\partial^2 v}{\partial y^2}\right)-\frac{\partial p}{\partial y}. \tag{32}$$

The non-dimensionalized equations look exactly like the dimensionalized ones. This implies that neither the viscous force nor the pressure force is dominant and the order of magnitude of each of them is about the same. In the case of the non-dimensionalized Navier–Stokes equations, the Reynolds number appears and the dominant physical phenomenon is governed by the magnitude of it, i.e. the higher the inertia force, the higher is the Reynolds number. If the Stokes equations are considered as a special case of the Navier–Stokes equations with the inertia term neglected, then the Reynolds number by its definition becomes zero and it is proper that it does not appear in the non-dimensionalized Stokes equations.

These field equations are used to solve the flow field with the boundary conditions that do not represent the stresses physically (see Appendix I). The forces and the viscous dissipation will be obtained using the appropriate formulae, namely equations (8) and (10).

4. NUMERICAL EXPERIMENTATION

4.1. Discretization of flow domain

The eight-noded isoparametric rectangular serendipity elements were chosen with mixed-order interpolation for velocity and pressure. The flow domain with the boundary conditions is shown in Figure 1. Since the flow is symmetric with respect to the mid-plane, only half the body and the associated flow domain is considered for solving the flow field. The inlet boundary is at a distance of five times the diameter of the semicircular body from the centre of the body and the exit boundary is at a distance of 10 times the diameter from the centre of the body. The third boundary parallel to the symmetry boundary is at a distance of 10 times the diameter from the centre of the body. This selection of boundaries simulates the far-field conditions fairly well.[8] Figure 2 shows the mesh discretization of the flow domain. As one can see, near the body the size of the elements is smaller to better resolve the gradients, and the size of the elements becomes gradually bigger in the outward radial direction until they merge with the checkerboard-type elements.

4.2.1. Flow over a semicircular body. The non-dimensionalized drag force and the energy dissipation rate are evaluated through separate subroutine subprogrammes and are post-processing operations carried out after solving for the flow field. The zoom-in view of the mesh closer to the body is shown in Figure 3, the streamline contour plot for the flow is shown in Figure 4, the pressure contour plot is shown in Figure 5 and the energy dissipation rate contour plot is shown in Figure 6. An interesting observation here is that the maximum energy dissipation rate occurs not on the surface of the body but in front of the body and behind the body, and very little energy dissipation occurs in the rest of the domain. It is worth pointing out that since unit velocity is specified in the x-direction (this is also the direction of drag) at the inlet, the value of the non-dimensionalized energy dissipation rate calculated should be equal to the value of the non-dimensionalized drag. The non-dimensionalized drag force was calculated as 69·9 (using equation (8) or the x-component of equation (17)) and the total non-dimensionalized energy

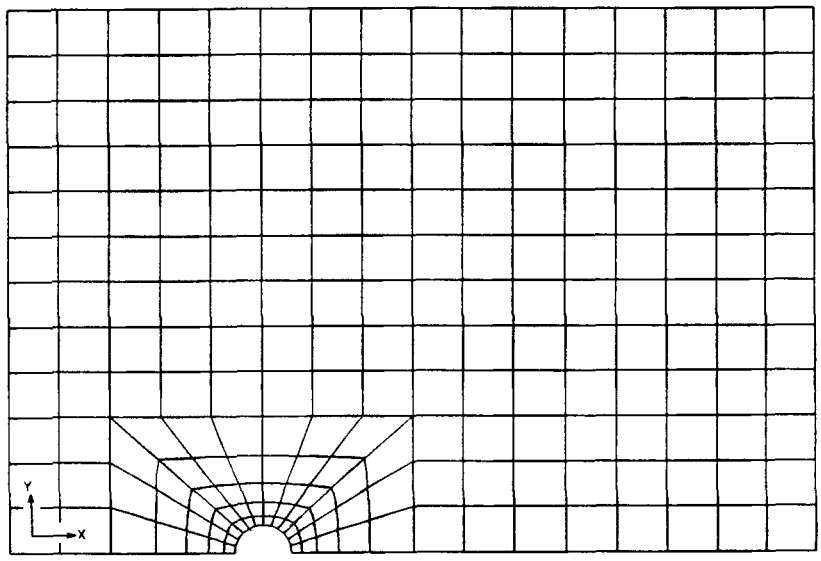

Figure 2. Mesh discretization of flow domain

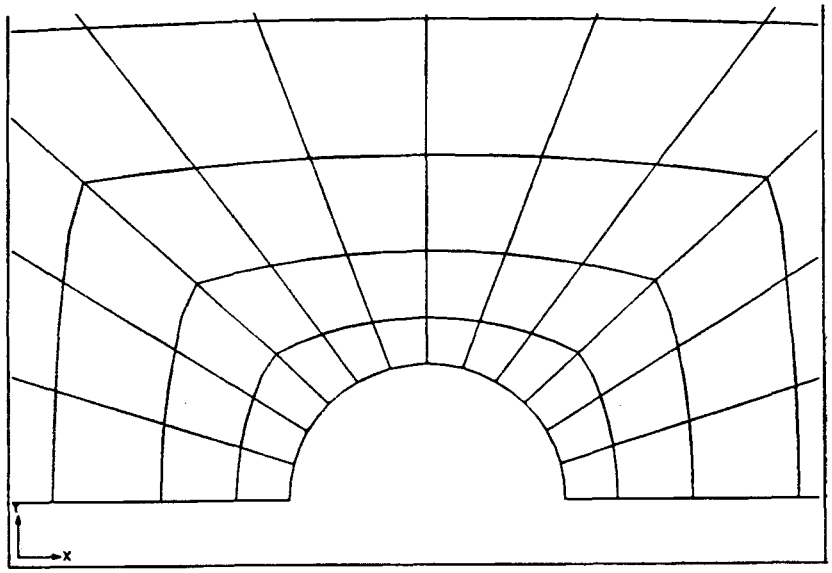

Figure 3. Zoom-in view of semicircular body

dissipation rate for the entire domain was calculated as 70·3 (using equation (10) for ϕ on the RHS of equation (27)), i.e. a difference of 0·57%. This is in accordance with the Stokes drag law.

4.2.2. Flow over a semi-ellipse. Next, the flow over an elliptic cross-section (with conical front and rear ends) with an area equal to that of the semicircle just considered was analysed. The

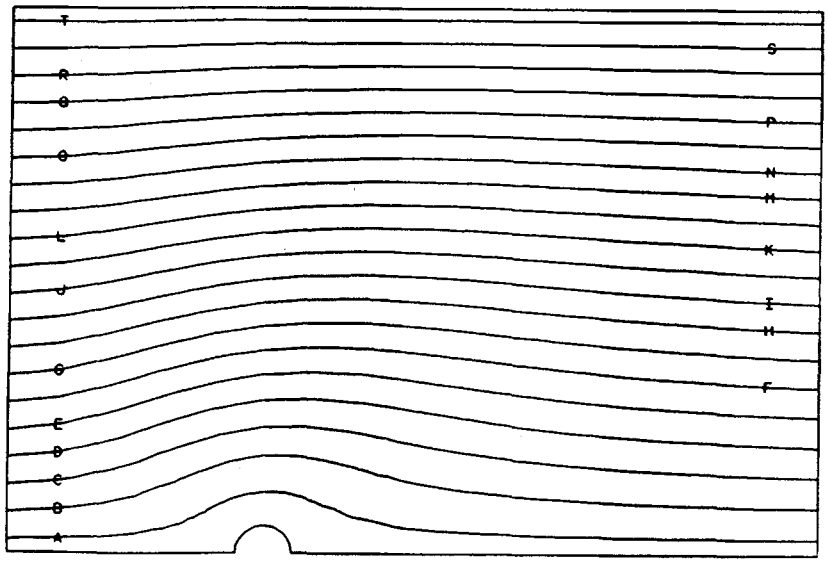

Figure 4. Streamlines for flow over a semicircle

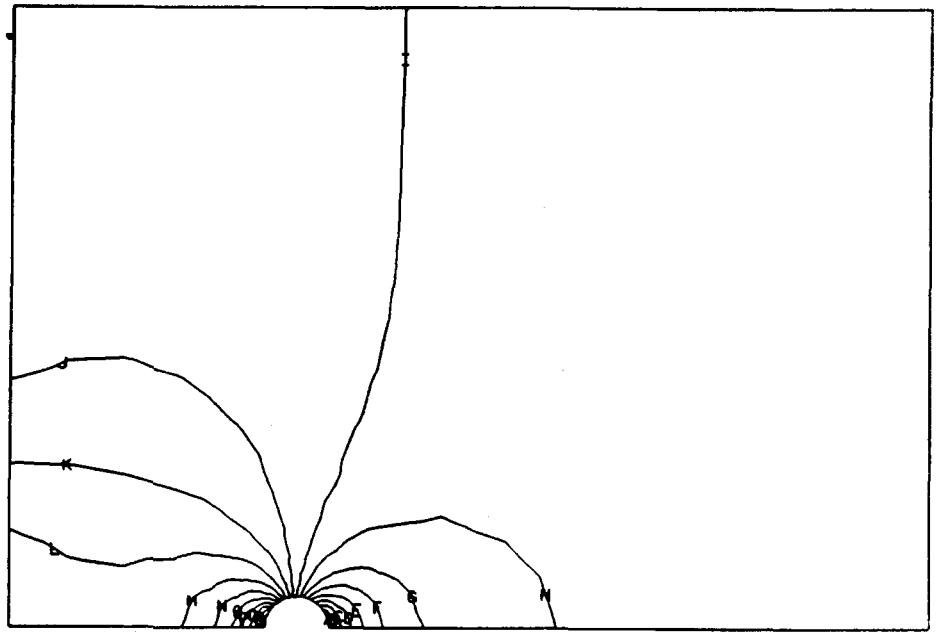

Figure 5. Pressure contours for flow over a semicircle

zoom-in view of the mesh closer to the body is shown in Figure 7 and the energy dissipation rate contour plot is shown in Figure 8. The values of non-dimensionalized drag and non-dimensionalized energy dissipation rate were calculated to be 66·9 and 67·5 respectively, i.e. a difference of 0·9%.

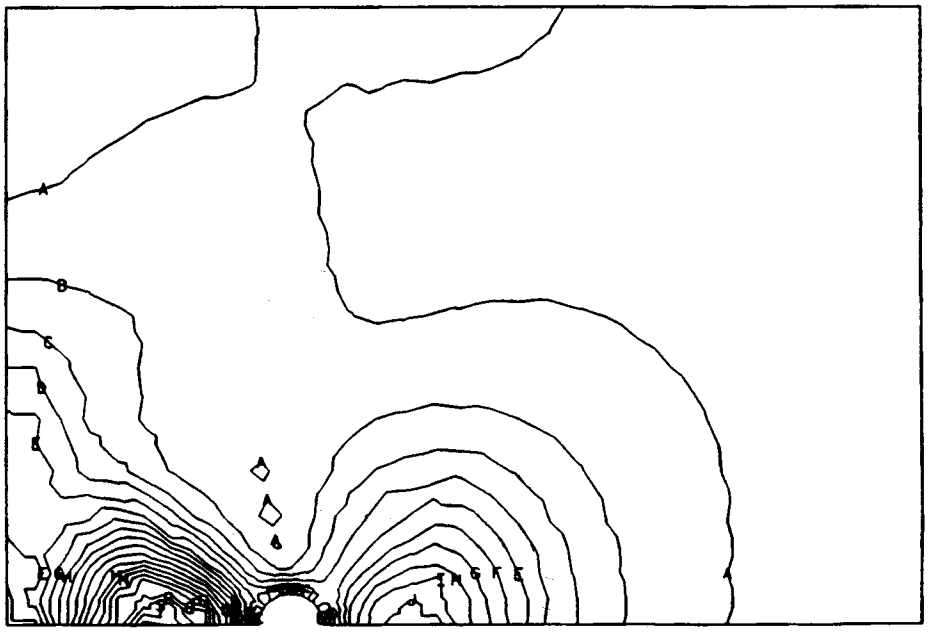

Figure 6. Energy dissipation rate contours for semicircle

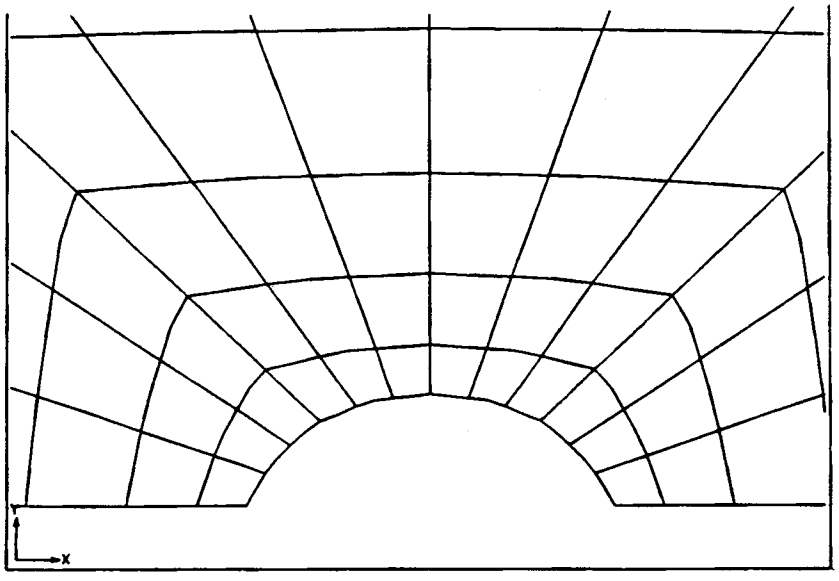

Figure 7. Zoom-in view of semi-elliptical body

4.2.3. Flow over a semi-prolate spheroidal cross-section. A prolate spheroidal cross-section was obtained by using the formula[9]

$$\frac{r(\theta)}{\lambda}=2-\frac{2}{\sqrt{3}}\sin\theta+\sum_{n=1}^{10}B_n\sin^{n+1}\theta, \tag{33}$$

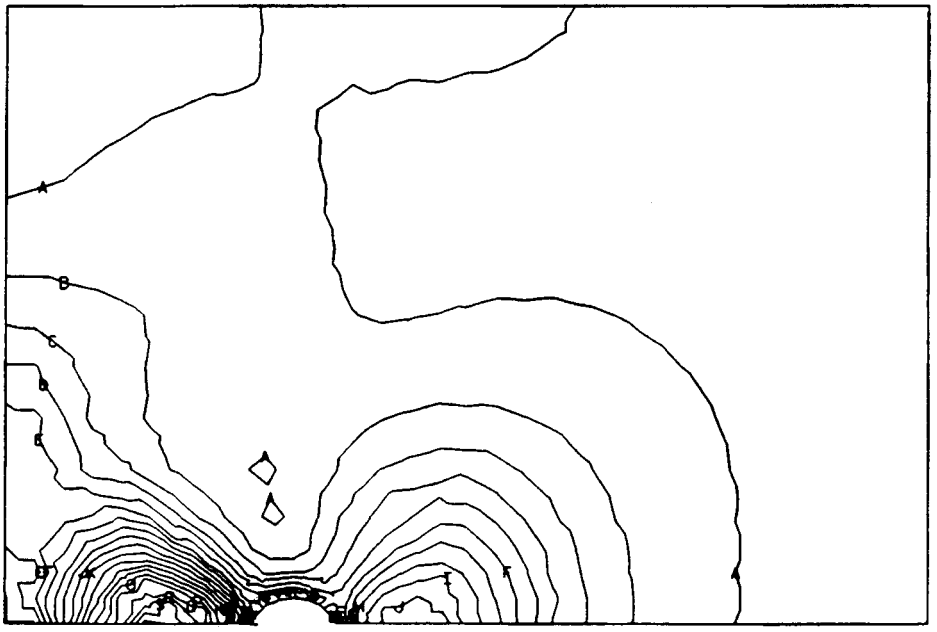

Figure 8. Energy dissipation rate contours for semi-ellipse

where r denotes the distance from the centre, θ is the co-altitude and λ is a scaling coefficient for area adjustment. A numerical routine was used to evolve this profile by adjusting λ in order to keep the area the same as that of the semicircle and semi-ellipse. The zoom-in view of the mesh closer to the body is shown in Figure 9. The energy dissipation contour plot is shown in Figure 10. The non-dimensionalized drag force and non-dimensionalized energy dissipation rate were calculated to be 65·8 and 66·2 respectively, i.e. a difference of 0·6%. Bourot[9] found that the drag on this optimal-shaped (prolate spheroid, 3D) body is 0·95425 times the drag on the sphere of equal volume. Here the drag for the 2D cross-section of the same body is found to be 0·94 times the drag on the circular cross-section of equal area.

4.3. General remarks

As can be seen, the energy dissipation rate contours shown are not symmetric with respect to the body. This is because not only is the domain unsymmetric but the boundary conditions are as well, as shown in Figure 1. Truly symmetric boundary conditions would mean the exit boundary has the same constrained velocity boundary conditions as the inlet. The boundary parallel to the symmetry boundary has in either case constrained velocity boundary conditions applied. The two combinations, i.e. unsymmetric boundary conditions on a symmetric domain and symmetric boundary conditions on an unsymmetric domain, produced unsymmetric contours. The perfectly symmetric contours shown in Figure 11 have been obtained only for a symmetric domain with symmetric boundary conditions, i.e. constrained velocities on the inlet, exit and the third boundary parallel to the symmetry boundary. It is worth pointing out that in all cases experimented, in spite of no symmetry (and with complete symmetry too), the Stokes drag law in 2D, equation (27), holds good. There is yet another important aspect that is worth investigating.

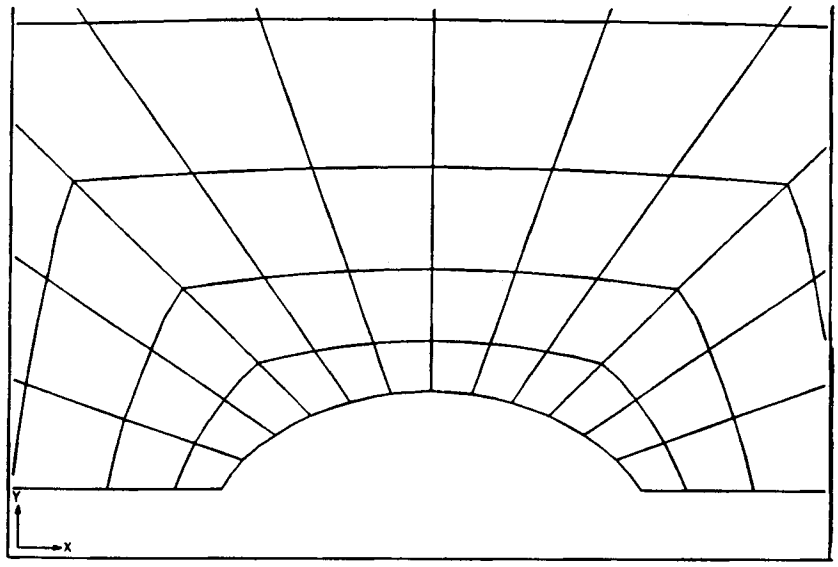

Figure 9. Zoom-in view of semi-prolate spheroidal cross-sectional body

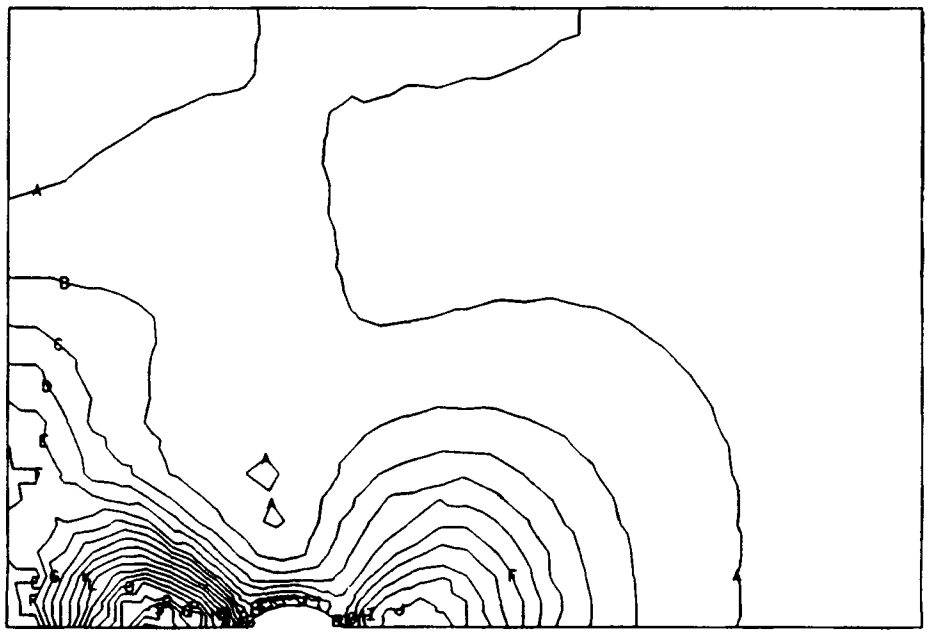

Figure 10. Energy dissipation rate contours for semi-prolate spheroidal cross-section

So far in the above experiments the body was held stationary and the fluid stream went past it. To see what happens when the body is moved in a quiescent fluid, the same experiments were conducted with the three aforementioned combinations of boundary conditions and domains and it was found that the energy dissipation rate contours, their magnitude and the drag were exactly

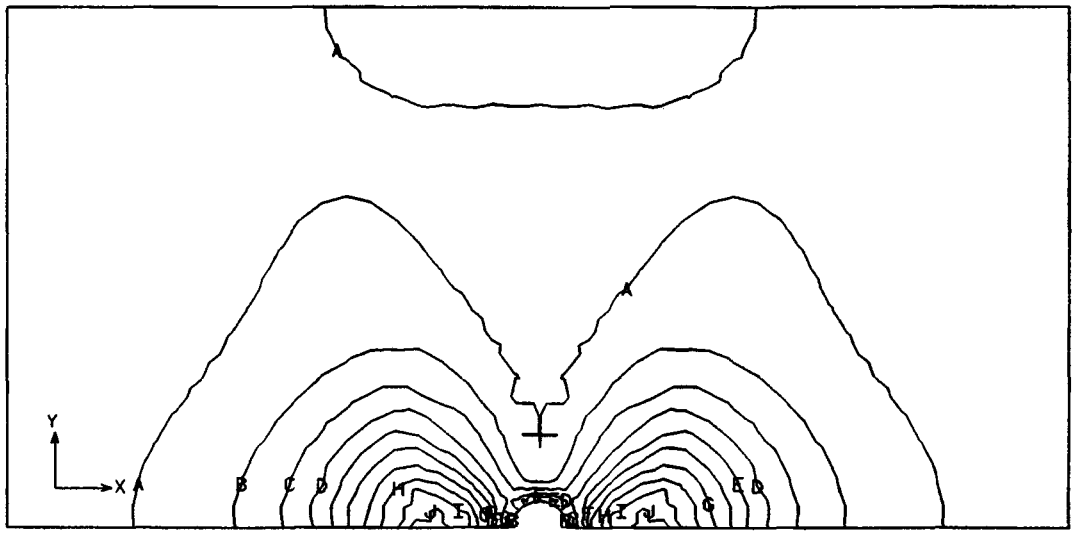

Figure 11. Energy dissipation rate contours for semicircle with symmetric domain

the same. However, the streamlines and the pressure contours were different. The relative motion and the drag are the same whether a body moves at uniform speed through a stagnant fluid or a large body of fluid streams past the body as in a wind tunnel. These two circumstances are equivalent. The change in viewing position of the stationary observer from one where he is attached to the body to one where he is attached to the flow is called a 'Galilean transformation'.[10]

It was mentioned before that the maximum energy dissipation rate occurs in front of and behind the body in 2D domains. To see what is happening in a 3D flow, the energy dissipation rate was calculated for a sphere using the expressions given in spherical co-ordinates.[1] It was found that the maximum occurs at equal distances both in front of and behind the sphere, confining the calculations to a plane. In the 2D domain for a circular cylinder also the maximum occurs at equal distances both in front of and behind the cylinder for a symmetric domain with symmetric boundary conditions. Since the 2D analysis differs from a 3D one, the distances are not the same despite observing similar trends.

Finally, the energy dissipation rate contours were obtained for finite Reynolds numbers of 10 and 20 and are shown in Figures 12 and 13 respectively. The energy dissipation rate contours are concentrated in the downstream wake region all the way up to the end of the domain. The global force and energy balances have been derived from first principles (our aim is to evaluate drag just as we did for Stokes flow) and it is observed that the difference between inertial flow and Stokes flow is the inclusion of the inertial force term in the force balance and the inertial power term in the energy balance. The inertial integral terms (see Appendix II) have been evaluated numerically using the FEM and, by making use of the generalized global energy equation, an alternative way to evaluate the drag numerically is again obtained in non-linear flow. Note that one has to evaluate the energy dissipation rate integral in addition to the inertia integrals. In the special case of Stokes flow this global energy equation collapses to the Stokes drag law when the inertial integral term is neglected.

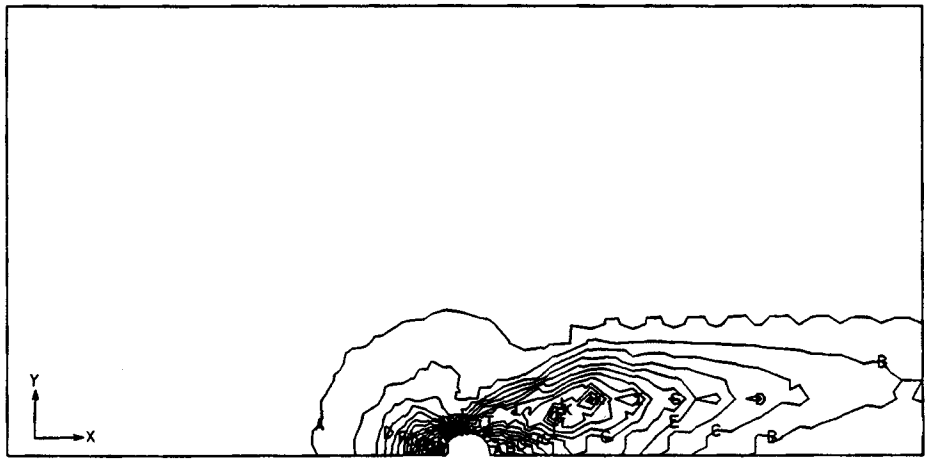

Figure 12. Energy dissipation rate contours for $Re = 10$

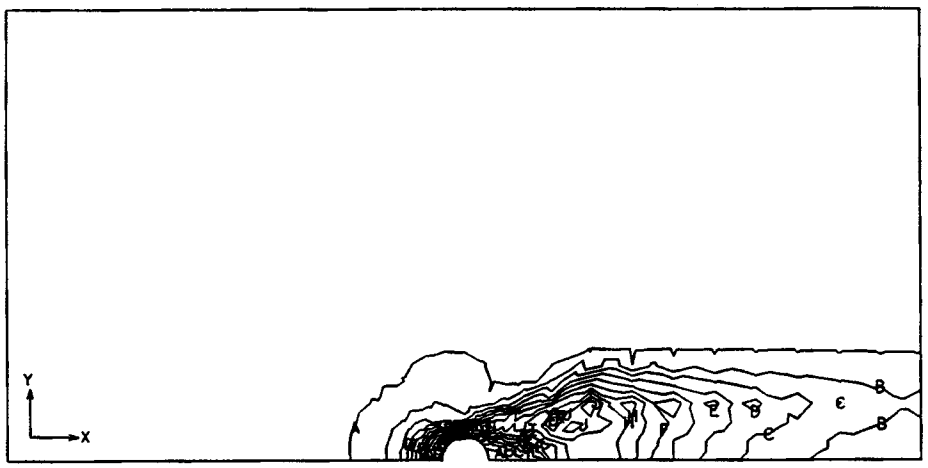

Figure 13. Energy dissipation rate contours for $Re = 20$

5. CLOSURE

A numerical method of evaluating the drag on a body from the total energy dissipation rate for a 2D domain is developed using the finite element technique of numerical integration. Eight-noded serendipity elements with mixed-order interpolation for velocity components and pressure were used in the analysis. It is shown here that the drag on an arbitrarily shaped body can be obtained by dividing the integrated energy dissipation rate in the entire flow domain by the uniform velocity at infinity. The flows over three different profiles—a semicircle, a semi-ellipse and a cross-section of a semi-prolate spheroid—were studied (the area remained the same). The subroutines developed were used in conjunction with the code developed by Taylor and Hughes.[11] Since this software did not have a post-processor with graphic facilities, only numerical values were

obtained. Another code, *FIDAP*[12] (courtesy of United Technologies Research Center), was used to study the flow over the same profiles and the results were compared and found to be in agreement. These results can also be construed as a numerical verification for the *Stokes drag law in 2D* and offer a justification for the use of the energy dissipation rate as a cost function in the minimum drag problem in Stokes flow. Another advantage of this verification method is that it offers an effective way to check the correctness of coding for the drag calculations.

ACKNOWLEDGEMENTS

The author wishes to express his thanks to Professor Wallace W. Bowley, Professor of Mechanical Enginnering, University of Connecticut for his advice and encouragement. The author is also indebted to Dr. Alan F. Haught, Manager (Thermal Science), United Technologies Research Center, East Hartford, CT, for permitting the author to use FIDAP[12] at UTRC (without which it would not have been possible to produce meshes and contours) and for his suggestions as well. The author thanks Dr. Phillip M. Gresho, Editor of *International Journal for Numerical Methods in Fluids*, Lawrence Livermore National Laboratory, Livermore, CA, for his suggestions, advice and co-operation in making this publication possible.

APPENDIX I: STOKES VERSUS STRESS-DIVERGENCE FE FORMULATION OF STOKES EQUATIONS

Stokes formulation

The Stokes equations are

$$\frac{\partial u}{\partial y}+\frac{\partial v}{\partial x}=0, \qquad \mu\left(\frac{\partial^2 u}{\partial x^2}+\frac{\partial^2 u}{\partial y^2}\right)=\frac{\partial p}{\partial x}, \qquad \mu\left(\frac{\partial^2 v}{\partial x^2}+\frac{\partial^2 v}{\partial y^2}\right)=\frac{\partial p}{\partial y}. \tag{34}$$

The Galerkin procedure applied at node i of an isolated element for the Stokes equations results in

$$\int_{\Omega_e} N_i[\mu(\nabla\cdot\nabla u^e-\nabla_x p^e)]\,d\Omega=0,$$

$$\int_{\Omega_e} N_i[\mu(\nabla\cdot\nabla v^e-\nabla_y p^e)]\,d\Omega=0,$$

$$\int_{\Omega_e} N_i^p(\nabla_x u^e+\nabla_y v^e)\,d\Omega=0, \tag{35}$$

where

$$u^e=\sum N_i(x,y)u_i, \qquad v^e=\sum N_i(x,y)v_i, \qquad p^e=\sum N_i^p(x,y)p_i. \tag{35a}$$

Applying Gauss theorem and vector calculus, we arrive at the following result for the x-momentum equation:

$$\int_{\Omega_e}\mu\nabla N_i\cdot\nabla u^e\,d\Omega-\int_{\Omega_e} p^e\nabla_x N_i\,d\Omega=\int_{\Gamma_e} N_i(\mu\nabla u^e\cdot\hat{\mathbf{n}}-n_x p^e)\,d\Gamma. \tag{36}$$

In Cartesian form,

$$\int_{\Omega_e} \mu\left(\frac{\partial N_i}{\partial x}\frac{\partial u^e}{\partial x}+\frac{\partial N_i}{\partial y}\frac{\partial u^e}{\partial y}\right)\mathrm{d}\Omega-\int_{\Omega_e}\frac{\partial N_i}{\partial x}p^e\,\mathrm{d}\Omega=\int_{\Gamma_e}N_i(\mu\nabla u^e\cdot\hat{\mathbf{n}}-n_x p^e)\,\mathrm{d}\Gamma. \tag{37}$$

The y-momentum equation can be derived in the same manner and the result is

$$\int_{\Omega_e} \mu\left(\frac{\partial N_i}{\partial x}\frac{\partial v^e}{\partial x}+\frac{\partial N_i}{\partial y}\frac{\partial v^e}{\partial y}\right)\mathrm{d}\Omega-\int_{\Omega_e}\frac{\partial N_i}{\partial y}p^e\,\mathrm{d}\Omega=\int_{\Gamma_e}N_i(\mu\nabla v^e\cdot\hat{\mathbf{n}}-n_y p^e)\,\mathrm{d}\Gamma. \tag{38}$$

When the approximate equations (35a) are substituted in the integral equations, the matrix equations for node i result as

$$\int_{\Omega_e} \mu\left(\frac{\partial N_i}{\partial x}\frac{\partial |N|}{\partial x}+\frac{\partial N_i}{\partial y}\frac{\partial |N|}{\partial y}\right)\mathrm{d}\Omega\,\{u\}-\int_{\Omega_e}\frac{\partial N_i}{\partial x}|N^p|\,\mathrm{d}\Omega\{p\}=\int_{\Gamma_e}N_i(\mu\nabla u^e\cdot\hat{\mathbf{n}}-n_x p^e)\,\mathrm{d}\Gamma, \tag{39}$$

$$\int_{\Omega_e} \mu\left(\frac{\partial N_i}{\partial x}\frac{\partial |N|}{\partial x}+\frac{\partial N_i}{\partial y}\frac{\partial |N|}{\partial y}\right)\mathrm{d}\Omega\,\{v\}-\int_{\Omega_e}\frac{\partial N_i}{\partial y}|N^p|\,\mathrm{d}\Omega\{p\}=\int_{\Gamma_e}N_i(\mu\nabla v^e\cdot\hat{\mathbf{n}}-n_y p^e)\,\mathrm{d}\Gamma, \tag{40}$$

where $|N|$ and $|N^p|$ are the velocity and pressure interpolation matrices. For the continuity equation the matrix equation becomes

$$\int_{\Omega_e} N_i^p\frac{\partial |N|}{\partial x}\,\mathrm{d}\Omega\,\{u\}+\int_{\Omega_e} N_i^p\frac{\partial |N|}{\partial y}\,\mathrm{d}\Omega\,\{v\}=0. \tag{41}$$

Now the element matrix equation can be written by inspection as

$$\begin{bmatrix} [K_1] & [0] & [K_2] \\ [0] & [K_1] & [K_3] \\ [K_4] & [K_5] & [0] \end{bmatrix}\begin{bmatrix} [u] \\ [v] \\ [p] \end{bmatrix}=\begin{bmatrix} [R_1] \\ [R_2] \\ [0] \end{bmatrix}, \tag{42}$$

where

$$K_{1ij}=\int_{\Omega_e}\mu\left(\frac{\partial N_i}{\partial x}\frac{\partial N_j}{\partial x}+\frac{\partial N_i}{\partial y}\frac{\partial N_j}{\partial y}\right)\mathrm{d}\Omega, \tag{43}$$

$$K_{2ij}=-\int_{\Omega_e}\frac{\partial N_i}{\partial x}N_j^p\,\mathrm{d}\Omega, \tag{44}$$

$$K_{3ij}=-\int_{\Omega_e}\frac{\partial N_i}{\partial y}N_j^p\,\mathrm{d}\Omega, \tag{45}$$

$$K_{4ij}=K_{2ji}, \tag{46}$$

$$K_{5ij}=K_{3ji}, \tag{47}$$

$$R_{1i}=\int_{\Gamma_e}N_i(\mu\nabla u^e\cdot\hat{\mathbf{n}}-n_x p^e)\,\mathrm{d}\Gamma, \tag{48}$$

$$R_{2i}=\int_{\Gamma_e}N_i(\mu\nabla v^e\cdot\hat{\mathbf{n}}-n_y p^e)\,\mathrm{d}\Gamma. \tag{49}$$

Stress-divergence formulation

The Stokes equations in the stress-divergence formulation[13] are

$$\frac{\partial u}{\partial x}+\frac{\partial v}{\partial y}=0, \qquad \frac{\partial(\sigma_x-p)}{\partial x}+\frac{\partial \tau_{xy}}{\partial y}=0, \qquad \frac{\partial \tau_{xy}}{\partial x}+\frac{\partial(\sigma_y-p)}{\partial y}=0, \tag{50}$$

where the stresses are related to the velocity components by

$$\sigma_x=2\mu\frac{\partial u}{\partial x}, \qquad \sigma_y=2\mu\frac{\partial v}{\partial y}, \qquad \tau_{xy}=\mu\left(\frac{\partial u}{\partial y}+\frac{\partial v}{\partial x}\right). \tag{51}$$

The Galerkin procedure applied at node i of an isolated element gives for the momentum equations and the continuity equation

$$\begin{aligned}\int_{\Omega_e}\left(\frac{\partial(\sigma_x-p)}{\partial x}+\frac{\partial \tau_{xy}}{\partial y}\right)N_i\,\mathrm{d}\Omega=0,\\ \int_{\Omega_e}\left(\frac{\partial \tau_{xy}}{\partial x}+\frac{\partial(\sigma_y-p)}{\partial y}\right)N_i\,\mathrm{d}\Omega=0,\\ \int_{\Omega_e}\left(\frac{\partial u}{\partial x}+\frac{\partial v}{\partial y}\right)N_i^p\,\mathrm{d}\Omega=0.\end{aligned} \tag{52}$$

If the momentum equations are integrated using Gauss theorem, we get

$$\int_{\Omega_e}\left[\left(2\mu\frac{\partial u}{\partial x}-p\right)\frac{\partial N_i}{\partial x}+\mu\left(\frac{\partial u}{\partial y}+\frac{\partial v}{\partial x}\right)\frac{\partial N_i}{\partial y}\right]\mathrm{d}\Omega=\int_{\Gamma_e}N_i\bar{\sigma}_x\,\mathrm{d}\Gamma, \tag{53a}$$

$$\int_{\Omega_e}\left[\mu\left(\frac{\partial u}{\partial y}+\frac{\partial v}{\partial x}\right)\frac{\partial N_i}{\partial x}+\left(2\mu\frac{\partial v}{\partial y}-p\right)\frac{\partial N_i}{\partial y}\right]\mathrm{d}\Omega=\int_{\Gamma_e}N_i\bar{\sigma}_y\,\mathrm{d}\Gamma, \tag{53b}$$

where

$$\bar{\sigma}_x=(\sigma_x-p)n_x+\tau_{xy}n_y, \qquad \bar{\sigma}_y=(\sigma_y-p)n_y+\tau_{xy}n_x. \tag{53c}$$

With the stress-divergence form of the momentum equations, the natural boundary conditions, i.e. the surface tractions, appear directly in the 'load' vector on the RHS. When the finite element approximation for the dependent variable is substituted in the above equation, the x-momentum matrix equation for node i results as

$$\begin{aligned}&\left[2\int_{\Omega_e}\mu\left(\frac{\partial N_i}{\partial x}\frac{\partial|N|}{\partial x}\right)\mathrm{d}\Omega+\int_{\Omega_e}\mu\left(\frac{\partial N_i}{\partial y}\frac{\partial|N|}{\partial y}\right)\mathrm{d}\Omega\right]\{u\}\\ &\quad+\int_{\Omega_e}\mu\left(\frac{\partial N_i}{\partial y}\frac{\partial|N|}{\partial x}\right)\mathrm{d}\Omega\,\{v\}-\int_{\Omega_e}\frac{\partial N_i}{\partial x}|N^p|\,\mathrm{d}\Omega\,\{p\}=\int_{\Gamma_e}N_i\bar{\sigma}_x\mathrm{d}\Gamma.\end{aligned} \tag{54}$$

The y-momentum matrix equation can be written similarly as

$$\begin{aligned}&\int_{\Omega_e}\mu\left(\frac{\partial N_i}{\partial x}\frac{\partial|N|}{\partial y}\right)\mathrm{d}\Omega\,\{u\}+\left[\int_{\Omega_e}\mu\left(\frac{\partial N_i}{\partial x}\frac{\partial|N|}{\partial x}\right)\mathrm{d}\Omega+2\int_{\Omega_e}\mu\left(\frac{\partial N_i}{\partial y}\frac{\partial|N|}{\partial y}\right)\mathrm{d}\Omega\right]\{v\}\\ &\quad-\int_{\Omega_e}\frac{\partial N_i}{\partial y}|N^p|\,\mathrm{d}\Omega\,\{p\}=\int_{\Gamma_e}N_i\bar{\sigma}_y\,\mathrm{d}\Gamma.\end{aligned} \tag{55}$$

The matrix equation for node i for the continuity equation is

$$\int_{\Omega_e} N_i^p \frac{\partial |N|}{\partial x} \, d\Omega \{u\} + \int_{\Omega_e} N_i^p \frac{\partial |N|}{\partial y} \, d\Omega \{v\} = 0. \tag{56}$$

From these equations, the element matrix equation can be written by inspection as

$$\begin{bmatrix} [K_1] & [K_7] & [K_3] \\ [K_8] & [K_2] & [K_4] \\ [K_5] & [K_6] & [0] \end{bmatrix} \begin{bmatrix} [u] \\ [v] \\ [p] \end{bmatrix} = \begin{bmatrix} [R_1] \\ [R_2] \\ [0] \end{bmatrix}, \tag{57}$$

where

$$K_{1ij} = \int_{\Omega_e} \mu \left[2\left(\frac{\partial N_i}{\partial x} \frac{\partial N_j}{\partial x} \right) + \left(\frac{\partial N_i}{\partial y} \frac{\partial N_j}{\partial y} \right) \right] d\Omega, \tag{58}$$

$$K_{2ij} = \int_{\Omega_e} \mu \left[\left(\frac{\partial N_i}{\partial x} \frac{\partial N_j}{\partial x} \right) + 2\left(\frac{\partial N_i}{\partial y} \frac{\partial N_j}{\partial y} \right) \right] d\Omega, \tag{59}$$

$$K_{3ij} = -\int_{\Omega_e} \frac{\partial N_i}{\partial x} N_j^p \, d\Omega, \tag{60}$$

$$K_{4ij} = -\int_{\Omega_e} \frac{\partial N_i}{\partial y} N_j^p \, d\Omega, \tag{61}$$

$$K_{5ij} = K_{3ji}, \tag{62}$$

$$K_{6ij} = K_{4ji}, \tag{63}$$

$$K_{7ij} = \int_{\Omega_e} \mu \left(\frac{\partial N_i}{\partial y} \frac{\partial N_j}{\partial x} \right) d\Omega, \tag{64}$$

$$K_{8ij} = K_{7ji}, \tag{65}$$

$$R_{1i} = \int_{\Gamma_e} N_i \bar{\sigma}_x \, d\Gamma, \tag{66}$$

$$R_{2i} = \int_{\Gamma_e} N_i \bar{\sigma}_y \, d\Gamma, \tag{67}$$

and $\bar{\sigma}_x$ and $\bar{\sigma}_y$ have been previously defined by equations (53c).

Thus it can be seen from the two formulations that the matrices and the right-hand sides are different. However, the solutions will differ only by a small amount owing to the difference in truncation error between equations (42) and (57) and the fact that the flow is incompressible. In the Stokes formulation the 'load' vectors will contain only velocity gradients (corresponding to $\gamma = 0$ in Appendix II), which do not represent stresses. In the stress-divergence formulation, however, the 'load' vectors do represent the stresses physically and this is conducive to physical interpretation (corresponding to $\gamma = 1$ in Appendix II). Regardless of how the flow field is obtained (the flow field could have been obtained using the Stokes formulation), it is always possible to calculate the stresses on any boundary using the appropriate stress formulae which represent the stresses physically, as a post-processing operation.

APPENDIX II: STRESS-DIVERGENCE, FORCES AND VISCOUS DISSIPATION

The Navier–Stokes equation in the stress-divergence form is

$$\rho \mathbf{U}\cdot\nabla\mathbf{U}=\nabla\cdot\boldsymbol{\sigma}(\gamma), \tag{68}$$

where

$$\boldsymbol{\sigma}(\gamma)\equiv\begin{bmatrix} -p+(1+\gamma)\mu\dfrac{\partial u}{\partial x} & \mu\left(\dfrac{\partial u}{\partial y}+\gamma\dfrac{\partial v}{\partial x}\right) \\ \mu\left(\gamma\dfrac{\partial u}{\partial y}+\dfrac{\partial v}{\partial x}\right) & -p+(1+\gamma)\mu\dfrac{\partial v}{\partial y}\end{bmatrix}$$

$$\equiv\boldsymbol{\Pi}(\gamma)-p\boldsymbol{I}; \tag{68a}$$

$\gamma=0$ gives the Navier–Stokes formulation and $\gamma=1$ gives the stress-divergence formulation. While these two forms are equivalent in the continuum, they are not (though very close) in the numerical approximations. The continuity equation is

$$\nabla\cdot\mathbf{U}=0. \tag{69}$$

Multiplying the momentum equation by $\mathbf{U}$ and integrating over the domain Ω gives

$$\begin{aligned}\int_\Omega p\mathbf{U}\cdot(\mathbf{U}\cdot\nabla\mathbf{U})\,d\Omega &= \int_\Omega \mathbf{U}\cdot(\nabla\cdot\boldsymbol{\sigma}(\gamma))\,d\Omega \\ &= \int_\Omega \nabla\cdot(\boldsymbol{\sigma}(\gamma)\cdot\mathbf{U})\,d\Omega-\int_\Omega \boldsymbol{\Pi}(\gamma):\nabla\mathbf{U}\,d\Omega+\int_\Omega p\boldsymbol{I}:\nabla\mathbf{U}\,d\Omega \\ &= \int_\Gamma \hat{\mathbf{n}}\cdot\boldsymbol{\sigma}(\gamma)\cdot\mathbf{U}\,d\Gamma-\int_\Omega \Phi(\gamma)\,d\Omega,\end{aligned} \tag{70}$$

where $\boldsymbol{I}:\nabla\mathbf{U}=\nabla\cdot\mathbf{U}=0$ and Φ is the energy dissipation rate. The traction vector on the boundary Γ is

$$\mathbf{F}_\gamma=\hat{\mathbf{n}}\cdot\boldsymbol{\sigma}(\gamma). \tag{71}$$

Thus, equation (70) becomes

$$\int_\Gamma \mathbf{F}_\gamma\cdot\mathbf{U}\,d\Gamma=\int_\Omega \rho\mathbf{U}\cdot(\mathbf{U}\cdot\nabla\mathbf{U})\,d\Omega+\int_\Omega \Phi(\gamma)\,d\Omega. \tag{72}$$

Splitting the boundary integral for each specific boundary and applying the boundary conditions of Figure 1,

$$u=U_\infty \quad\text{and}\quad v=0 \quad\text{on } \Gamma_{\text{inlet}},$$

$$u=U_\infty \quad\text{and}\quad v=0 \quad\text{on } \Gamma_{\text{top}},$$

$$\frac{\partial u}{\partial y}+\gamma\frac{\partial v}{\partial x}=0 \quad\text{and}\quad v=0 \quad\text{on } \Gamma_{\text{symm}},^*$$

$$-p+(1+\gamma)\mu\frac{\partial u}{\partial x}=0 \quad\text{and}\quad \gamma\frac{\partial u}{\partial y}+\frac{\partial v}{\partial x}=0 \quad\text{on}\quad \Gamma_{\text{exit}},^*$$

$$u=0 \quad\text{and}\quad v=0 \quad\text{on } \Gamma_0, \text{ the body boundary,}$$

* The actual boundary conditions shown in Figure 1 are with $\gamma=0$. However, only when $\gamma=1$ do these expressions represent the stresses; and for solving for the flow field refer to Appendix I.

we get

$$\int_\Gamma \mathbf{F}_\gamma \cdot \mathbf{U}\,d\Gamma = \int_{\Gamma_0} \mathbf{F}_\gamma \cdot \mathbf{U}\,d\Gamma + \int_{\Gamma_{inlet}} \mathbf{F}_\gamma \cdot \mathbf{U}\,d\Gamma + \int_{\Gamma_{top}} \mathbf{F}_\gamma \cdot \mathbf{U}\,d\Gamma + \int_{\Gamma_{symm}} \mathbf{F}_\gamma \cdot \mathbf{U}\,d\Gamma + \int_{\Gamma_{exit}} \mathbf{F}_\gamma \cdot \mathbf{U}\,d\Gamma$$

$$= \int_{\Gamma_{inlet}} U_\infty \left(-p + (1+\gamma)\mu \frac{\partial u}{\partial x} \right) d\Gamma + \int_{\Gamma_{top}} U_\infty \mu \left(\frac{\partial u}{\partial y} + \gamma \frac{\partial v}{\partial x} \right) d\Gamma$$

$$+ \int_{\Gamma_{symm}} u \left(\frac{\partial u}{\partial y} + \gamma \frac{\partial v}{\partial x} \right) d\Gamma + \int_{\Gamma_{exit}} u \left(-p + (1+\gamma)\mu \frac{\partial u}{\partial x} \right) d\Gamma$$

$$+ \int_{\Gamma_{exit}} v \left(\gamma \frac{\partial u}{\partial y} + \frac{\partial v}{\partial x} \right) d\Gamma$$

$$= U_\infty \int_{\Gamma_{inlet}} \left(-p + (1+\gamma)\mu \frac{\partial u}{\partial x} \right) d\Gamma + U_\infty \int_{\Gamma_{top}} \mu \left(\frac{\partial u}{\partial y} \right) d\Gamma$$

$$= \mathbf{U}_\infty \cdot \int_{\Gamma_{inlet}} \mathbf{F}_\gamma \, d\Gamma + \mathbf{U}_\infty \cdot \int_{\Gamma_{top}} \mathbf{F}_\gamma \, d\Gamma. \tag{73}$$

Therefore, it follows from equations (72) and (73) that

$$\mathbf{U}_\infty \cdot \int_{\Gamma_{inlet}} \mathbf{F}_\gamma \, d\Gamma + \mathbf{U}_\infty \cdot \int_{\Gamma_{top}} \mathbf{F}_\gamma \, d\Gamma = \int_\Omega \rho \mathbf{U} \cdot (\mathbf{U} \cdot \nabla \mathbf{U})\, d\Omega + \int_\Omega \Phi(\gamma)\, d\Omega. \tag{74}$$

This equation is true only for $\gamma = 1$, when $\mathbf{F}_\gamma$, the force, and Φ, the energy dissipation rate, are true physical quantities. The total reactive force exerted by the body on the fluid is given by

$$\mathbf{F} = \int_{\Gamma_0} \boldsymbol{\sigma}(1) \cdot \hat{\mathbf{n}}\, d\Gamma$$

$$= \int_{\Gamma_0} \mathbf{F}_1 \, d\Gamma, \tag{75}$$

and

$$\mathbf{U}_\infty \cdot \mathbf{F} = U_\infty \int_{\Gamma_0} F_{x1} \, d\Gamma$$

$$= U_\infty D, \tag{76}$$

where D is the magnitude of the drag force parallel to the relative approach velocity $\mathbf{U}_\infty$. Integrating the Navier–Stokes equation over the domain Ω,

$$\int_\Omega \rho(\mathbf{U} \cdot \nabla \mathbf{U})\, d\Omega = \int_\Omega (\nabla \cdot \boldsymbol{\sigma}(\gamma))\, d\Omega$$

$$= \int_\Gamma \boldsymbol{\sigma}(\gamma) \cdot \hat{\mathbf{n}}\, d\Gamma$$

$$= \int_\Gamma \mathbf{F}_\gamma \, d\Gamma. \tag{77}$$

Forming the scalar product with $\mathbf{U}_\infty$,

$$\mathbf{U}_\infty \cdot \int_\Omega \rho(\mathbf{U}\cdot\nabla\mathbf{U})\,d\Omega = \mathbf{U}_\infty \cdot \int_\Gamma \mathbf{F}_\gamma\,d\Gamma$$
$$= \mathbf{U}_\infty \cdot \int_{\Gamma_0} \mathbf{F}_\gamma\,d\Gamma + \mathbf{U}_\infty \cdot \int_{\Gamma_{inlet}} \mathbf{F}_\gamma\,d\Gamma + \mathbf{U}_\infty \cdot \int_{\Gamma_{top}} \mathbf{F}_\gamma\,d\Gamma$$
$$+ \mathbf{U}_\infty \cdot \int_{\Gamma_{symm}} \mathbf{F}_\gamma\,d\Gamma + \mathbf{U}_\infty \cdot \int_{\Gamma_{exit}} \mathbf{F}_\gamma\,d\Gamma. \tag{78}$$

Using the boundary conditions and the orientations (the direction cosines) of the boundaries, the first term on the RHS becomes

$$\mathbf{U}_\infty \cdot \int_{\Gamma_0} \mathbf{F}_\gamma\,d\Gamma = U_\infty \int_{\Gamma_0} F_{x\gamma}\,d\Gamma$$
$$= U_\infty \int_{\Gamma_0} \left[\left(-p+(1+\gamma)\mu\frac{\partial u}{\partial x}\right)n_x + \mu\left(\frac{\partial u}{\partial y}+\gamma\frac{\partial v}{\partial x}\right)n_y\right]d\Gamma$$
$$= \mathbf{U}_\infty \cdot \mathbf{D} \quad (\text{if } \gamma = 1). \tag{79}$$

The fourth integral term on the RHS of equation (78) becomes

$$\mathbf{U}_\infty \cdot \int_{\Gamma_{symm}} \mathbf{F}_\gamma\,d\Gamma = U_\infty \int_{\Gamma_0} \left[\left(-p+(1+\gamma)\mu\frac{\partial u}{\partial x}\right)\overset{0}{\uparrow}n_x + \mu\left(\frac{\partial u}{\partial y}\overset{0}{\uparrow}+\gamma\frac{\partial v}{\partial x}\right)n_y\right]d\Gamma$$
$$= 0, \tag{80}$$

and the fifth integral term on the RHS of equation (78) becomes

$$\mathbf{U}_\infty \cdot \int_{\Gamma_{exit}} \mathbf{F}_\gamma\,d\Gamma = U_\infty \int_{\Gamma_{exit}} \left[\left(-p+(1+\gamma)\overset{0}{\uparrow}\mu\frac{\partial u}{\partial x}\right)n_x\right]d\Gamma. \tag{81}$$
$$= 0.$$

By virtue of equations (74), (80) and (81), equation (78) becomes

$$\mathbf{U}_\infty \cdot \int_\Omega \rho(\mathbf{U}\cdot\nabla\mathbf{U})\,d\Omega = \int_\Omega \rho\mathbf{U}\cdot(\mathbf{U}\cdot\nabla\mathbf{U})\,d\Omega + \int_\Omega \Phi(\gamma)\,d\Omega + U_\infty \int_{\Gamma_0} F_{x\gamma}\,d\Gamma. \tag{82}$$

Rearranging,

$$U_\infty \int_{\Gamma_0} F_{x\gamma}\,d\Gamma = \int_\Omega \rho(\mathbf{U}_\infty - \mathbf{U})\cdot(\mathbf{U}\cdot\nabla\mathbf{U})\,d\Omega - \int_\Omega \Phi(\gamma)\,d\Omega. \tag{83}$$

Therefore we can write, using equation (76),

$$U_\infty D = \int_\Omega \rho(\mathbf{U}_\infty - \mathbf{U})\cdot(\mathbf{U}\cdot\nabla\mathbf{U})\,d\Omega - \int_\Omega \Phi(\gamma)\,d\Omega + U_\infty \int_{\Gamma_0} (F_{x1} - F_{x\gamma})\,d\Gamma, \tag{84}$$

where

$$F_{x1} - F_{x\gamma} = \mu(1-\gamma)\left(n_x \frac{\partial u}{\partial x} + n_y \frac{\partial v}{\partial x}\right). \tag{84a}$$

If $\gamma = 1$, the above expression is zero and equation (84) becomes

$$U_\infty D = \int_\Omega \rho(\mathbf{U}_\infty - \mathbf{U}) \cdot (\mathbf{U} \cdot \nabla \mathbf{U})\, d\Omega - \int_\Omega \Phi(\gamma)\, d\Omega. \tag{85}$$

Only when $\gamma = 1$ do both $\Phi(\gamma)$ and $\mathbf{F}_\gamma$ represent the viscous dissipation and the force respectively. Equation (85) can be used to evaluate the drag in the steady non-linear flow over a body. Note that the magnitude of the drag force, which is a boundary quantity, is evaluated in terms of domain integrals. Equation (85) collapses to the one derived for Stokes flow if the inertial integral term is neglected.

REFERENCES

1. R. B. Bird, W. E. Stewart and E. N. Lightfoot, *Transport Phenomena*, Wiley, New York, 1960, pp. 82, 133 and 731.
2. S. F. Hoerner, *Fluid Dynamic Drag, Practical Information on Aerodynamic Drag and Hydrodynamic Resistance*, published by author, 1965.
3. O. Pironneau, 'On optimum profiles in Stokes flow', *J. Fluid Mech.*, **59**, 117–128 (1973).
4. J. Happel and H. Brenner, *Low Reynolds Number Hydrodynamics*, Martinus Nijhoff, Dordrecht/Boston/Lancaster, 1986, p. 47.
5. Y. C. Fung, *A First Course in Continuum Mechanics*, 2nd edn, Prentice-Hall, Englewood Cliffs, NJ, 1977, p. 70.
6. R. Panton, *Incompressible flow*, Wiley, New York, 1984, pp. 642–644.
7. J. Serrin, in S. Flugge (ed.) and C. Truedell (co-ed.), *Mathematical Principles of Classical Fluid Mechanics, Section 9 & 10; Handbuch der Physik, Vol. VIII/1, Fluid Dynamics 1*, Springer, Berlin/Gottingen/Heidelberg, 1959, pp. 138–139.
8. C. Taylor and P. Hood, 'A numerical solution of the Navier–Stokes equations using the finite element technique', *Comput. Fluids*, **1**, 73–100 (1973).
9. J. M. Bourot, 'On the numerical computation of the optimum profile in Stokes flow', *J. Fluid Mech.*, **65**, 513–515 (1974).
10. A. H. Shapiro, *Shape and Flow, the Fluid Dynamics of Drag, Science Study Series*, Anchor, Books, Garden City, NY, p. 26.
11. C. Taylor and T. G. Hughes, *Finite Element Programming of the Navier–Stokes Equations*, Pineridge Press Ltd., Swansea, U.K., 1981.
12. *FIDAP, Rev. 4.0*, Fluid Dynamics International, Evanston, IL, 1986.
13. K. H. Huebner and E. A. Thornton, *The Finite Element Methods for Engineers*, Wiley, New York, 1982, pp. 374–378.